Water Exclusion at the Nanometer Scale Provides Long-Term Passivation of Silicon (111) Grafted with Alkyl Monolayers

P. Gorostiza,[†,⊥] C. Henry de Villeneuve,[†] Q. Y. Sun,[†,#] F. Sanz,[‡] X. Wallart,[§] R. Boukherroub,[∥] and P. Allongue*[,†]

Laboratoire de Physique de la Matière Condensée, UMR 7643 CNRS, Ecole Polytechnique, Route de Saclay, F-91128 Palaiseau, France, Laboratory of Electrochemistry and Materials, University of Barcelona, Martí i Franquès 1, 08028 Barcelona, Spain, IEMN, CNRS−UMR 8520, B.P. 69, 59652 Villeneuve d'Ascq Cedex, France, and IRI−IEMN, Avenue Poincaré, B.P. 69, 59652 Villeneuve d'Ascq Cedex, France

Received: August 26, 2005; In Final Form: January 9, 2006

This work is a quantitative study of the conditions required for a *long-term* passivation of the interface silicon−alkyl monolayers prepared by thermal hydrosilyation of neat 1-alkenes on well-defined H−Si(111) surfaces. We present electrochemical capacitance measurements (*C*−*U*) in combination with ex situ atomic force microscopy (AFM) observations and X-ray photoelectron spectroscopy (XPS) measurements. Capacitance measurements as a function of the reaction time and XPS data reveal close correlations between the chemical composition at the interface and its electronic properties. A very low density of states is found if suboxide formation is carefully prevented. The monitoring of *C*−*U* plots and AFM imaging upon exposure of the sample in diverse conditions indicate that the initial electronic properties and structure of the interface are long-lasting only when the monolayer surface coverage is $\theta > 0.42$. A model demonstrates that this threshold value corresponds to a monolayer with intermolecular channels narrower than ∼2.82 Å, which is equal to the diameter of a water molecule. Water exclusion from the monolayer promotes long-term passivation of the silicon surface against oxidation in air and water as well as perfect corrosion inhibition in 20% NH_4F. We provide two criteria to assess when a sample is optimized: The first one is an effective dielectric constant <2.5, and the second one is a very characteristic energy diagram at open circuit potential.

1. Introduction

Organic monolayers directly anchored onto silicon substrates via reactions in a liquid phase are receiving increasing interest in view of future applications in microelectronics and bioelectronics.[1,2] The strong covalent bonding (e.g., Si−C, Si−O−C linkages) between the substrate and the molecules makes them very stable even in stringent conditions,[3] which constitutes a key advantage by comparison with self-assembled monolayers (SAMs) of *n*-alkanethiols on gold surfaces whose stability seems not as good and depends on several factors.[4] Because of the formation of energetic bonds (the energy of a Si−C bond is ∼4.5 eV) the layer growth cannot be assimilated to a self-assembling process since the anchored molecules have a small probability of desorption under mild reaction conditions. In that case the grafting is mainly a random nucleation stage with nearly no lateral domain growth, which explains why organic monolayers on silicon are thought to be disordered or to present only small molecular domains.[1] At room temperature, one noticeable exception is the phenyl monolayers grown on Si(111) by electrochemical reduction of a diazonium salt for which π-stacking is probably responsible for the development of wider molecular domains.[5] A recent sum frequency generation (SFG) study, in the case of alkyl monolayers prepared by thermal reaction at 200 °C, also showed that the alkyl chains adopt an all-trans configuration with surface ordering.[6] As a consequence of the grafting process the built-in defects are *punctual* defects (molecular vacancies) rather than extended defects (grain boundaries) at the modified silicon surfaces. This is an advantage, since a spatially *uniform* behavior is more likely than in the case of SAMs on Au(111) for which grain boundaries between the molecular domains play a significant role.[7] Minimizing the size and the density of defects in the monolayers grafted on silicon remains nevertheless essential to passivate the interface over the long term or, in other words, to prevent oxide uptake and to keep the initially low density of the interface states.[5,8,9] The design of reliable biological or chemical field effect transistor (FET) sensors, whose principle is based on the detection of changes in the surface charge,[10] requires reducing the influence of any unwanted or uncontrolled potential-induced charging at the substrate−organic layer interface.[11]

While the chemical stability or the robustness of organic layers on silicon were extensively studied in the past, the question of the interface integrity, in terms of chemical composition and electronic properties, has been rarely addressed. It is the purpose of this work to investigate quantitatively this crucial point using, as a model system, alkyl monolayers grafted via mild hydrosilylation of 1-alkenes on H−Si(111). We particularly paid attention to the grafting conditions (time and

* Author to whom correspondence should be addressed. Phone: +33 1 69334431. Fax: +33 1 69333004. E-mail: Philippe.Allongue@Polytechnique.fr.

† Laboratoire de Physique de la Matière Condensée, UMR 7643 CNRS, Ecole Polytechnique.

‡ Laboratory of Electrochemistry and Materials, University of Barcelona.

§ IEMN, CNRS−UMR 8520.

∥ IRI−IEMN.

⊥ Present address: Helen Wills Neuroscience Institute, University of California at Berkeley, Berkeley, CA 94720.

Permanent address: College of Chemistry and Chemical Engineering, Lanzhou University, Lanzhou, China.

10.1021/jp054825c CCC: $33.50
Published on Web 02/28/2006

temperature) to maximize the molecular density and to control the interface chemistry. Moreover, to keep full control on the system at the nanometer scale, the monolayers were prepared onto well-defined stepped H−Si(111) surfaces with atomically smooth terraces to ensure that the reported measurements are only a characteristic of the monolayer density and are not influenced by the initial surface state. The samples modified with an alkyl monolayer were characterized by in situ electrochemical capacitance ($C-U$) and open circuit potential (OCP) measurements in combination with ex situ atomic force microscopy (AFM) and X-ray photoelectron spectroscopy (XPS) measurements. Results indicate that achieving water exclusion at the nanometer scale is a prerequisite for the long-term passivation of the silicon surface in diverse conditions. Under this condition, which requires obtaining a surface coverage $\theta > 0.42$, the grafted silicon samples resist oxidation in air and water and therefore keep their initially excellent interface properties. Moreover the monolayer efficiently protects the surface against dissolution in 20% NH_4F. We provide two experimental criteria, the first one in terms of the effective dielectric constant and the second one in terms of the band diagram, to assess whether a sample is really optimized or not.

2. Experimental Section

2.1. Monolayer Formation. The alkyl monolayers can be realized by various hydrosilylation routes including thermal, catalytic, or photochemical activation by reaction of 1-alkenes with hydrogen-passivated silicon systems.[12−21] In this work we used a mild thermal hydrosilylation of 1-alkenes, in the presence of $C_2H_5AlCl_2$ as Lewis acid catalyst. The overall reaction may be written as[16]

$$\equiv Si-H + H_2C{=}CH-(CH_2)_{n-3}-CH_3 \rightarrow \equiv Si-(CH_2)_{n-1}-CH_3 \quad (1)$$

According to this reaction the anchoring of alkyl chains is expected via a Si−C linkage. The samples will be hereafter designated as $\equiv Si-C_n$ ($8 < n < 16$), where n is the number of carbon atoms in the chain. In practice, neat alkene (as purchased from Aldrich) was introduced in a Schlenk tube, flushed with N_2, and heated at 100 °C to eliminate oxygen and water traces. After the alkene was cooled to room temperature (still under N_2), 10 vol % of a 1 M $C_2H_5AlCl_2$ solution (1 M in hexane) was added, and the freshly prepared H−Si sample was introduced under N_2. The reactor was finally hermetically sealed, and the reaction was performed at 90 °C. At the end of the process, the reactor was cooled and opened to the air, and the samples immediately were rinsed with CF_3COOH (2% in THF) to neutralize residual $C_2H_5AlCl_2$ and then washed with high-performance liquid chromatography (HPLC) grade tetrahydrofuran (THF) and 1,1,1-trichloroethane (TCE). The sample was finally blown dry with a N_2 stream.

2.2. H−Si(111) Surface Preparation. The silicon samples were cut from 10 Ω cm n-type Si(111) wafers with a 0.2° miscut angle along $\langle 1\bar{1}2\rangle$, as purchased from Siltronix (France). After being cleaned in hot H_2SO_4 (95%)/H_2O_2 (30%) (2:1 in volume) mixture, followed by a copious rinse with 18.2 MΩ cm water, the sample was immersed for 15 min in VLSI grade 40% NH_4F containing 50 mM $(NH_4)_2SO_3$ as an oxygen scavenger to obtain an atomically smooth surface with no etch pits.[22] A quick rinse with water was finally performed to remove adventitious residues of etching. Thus prepared surfaces exhibit atomically smooth (111) terraces separated by monatomic steps (see AFM observations), which are fully hydrogen-terminated as derived from Fourier transform IR spectroscopy (not shown). The low miscut angle and its precise orientation toward $\langle 1\bar{1}2\rangle$ allows a staircase structure to be obtained (Figure 6), with a very low density of structural defects (step edges and kink sites), so that the properties measured in this work are characteristic of the modified interface and are not affected by some preexisting surface imperfections.

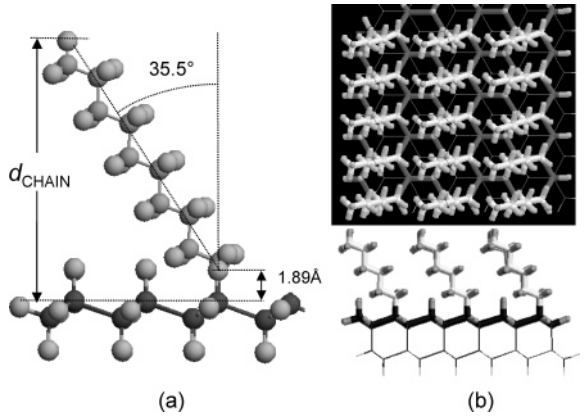

Figure 1. (a) Optimized ball-and-stick model of a silicon cluster with one decyl chain. The tilt angle is 35.5° from the surface normal, and d_{CHAIN} is the chain length projected on the surface normal. Equation 2 gives the expression of d_{CHAIN}. (b) Optimized model (top and side views) in the case of a 0.5 surface coverage. The 15 chains were anchored so as to build a 2×1 structure. Note the absence of any deformation of the on the silicon slab.

2.3. Structural Modeling of the Interface. In Figure 1 we present ball-and-stick models of the silicon−molecule interface calculated from Alchemy III software (Tripos). The bond lengths and angles are optimized around an imposed initial configuration, taking into account van der Waals interactions. The ideal configuration of the alkyl chain is all-trans, as shown in Figure 1a, in agreement with more sophisticated molecular dynamics simulations[23] and with SFG measurements.[6] The tilt angle is 35.5° from the surface normal. In the case of a chain with an *even* number n of carbon atoms, the projection d_{CHAIN} of its length on the surface normal is given by

$$d_{CHAIN}(\text{Å}) = 1.89 + (n/2 - 1)2.54 \cos 35.5° + 1.56 \sin 19° + 1.1 \quad (2)$$

The different bond lengths were obtained from the simulations. Figure 1b shows a slab consisting in a silicon bilayer (to keep the slab rigid) with 15 chains (C6) and 15 Si−H bonds for a 50% occupancy of the surface. Both the top and the side views of the slab confirm that such a close packing is perfectly attainable, as previously reported,[23] since there is no evidence of any deformation of the silicon bilayer. The top view shows also that the chains remain close packed even at the edges of the slab, which is an indication that the van der Waals interactions are accounted for. The measured chain tilt is 35.5° as in Figure 1a. At much lower surface coverages, we cannot exclude that the aliphatic chains adopt a different configuration, for instance, with a greater tilt. This case is not considered however in the following.

2.4. Atomic Force Microscopy. The topography of H−Si(111) and modified Si surfaces was checked using contact mode AFM (PicoSPM from Molecular Imaging, Phoenix, AZ) in a nitrogen atmosphere. Standard Si_3N_4 cantilevers with spring constants of 0.12 N m^{-1} (Nanoprobes) were employed.

2.5. Electrochemical Capacitance Measurements. The capacitance measurements were carried out using a three-

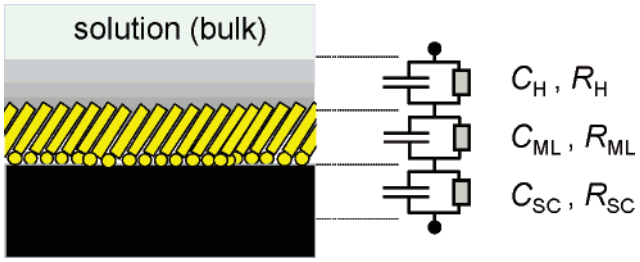

Figure 2. Equivalent circuit used to analyze the impedance data. The different parallel (R, C) elements correspond to the space charge region of the silicon substrate (R_{SC}, C_{SC}), the monolayer (R_{ML}, C_{ML}), and the Helmholtz layer (R_H, C_H).

electrode electrochemical cell connected to a potentiostat coupled with a frequency response analyzer (PGSTAT 10, Eco-Chemie, The Netherlands). A Pt grid and a hydrogen-loaded Pd wire served, respectively, as counter and quasi-reference electrodes. The potential of the quasi-reference electrode was measured with respect to a saturated sulfate mercury electrode (MSE) via a Teflon capillary junction. All potentials are quoted versus MSE. The ohmic contact at the rear side of the silicon sample was ensured by applying an InGa eutectic after mechanical removal (grinding) of the organic film.

The equivalent circuit of the interface is given in Figure 2. The different parallel (R, C) elements correspond to the space charge region of the silicon substrate (R_{SC}, C_{SC}), the monolayer (R_{ML}, C_{ML}), and the Helmholtz layer (R_H, C_H). The resistors account for the direct electrochemical current flow through the interface. As shown below the capacitance−voltage ($C-U$) plots under cathodic bias present a saturation plateau whose height is frequency-independent in the 1−10 kHz range (Supporting Information, Figure S1). The plateau extends toward more negative potentials at larger frequencies because of the lower influence of the parallel resistors. All plots given in this paper correspond to a frequency of 1 kHz. The complete calculation of $C-U$ plots was performed as exposed elsewhere.[5,8] According to Figure 2 the equivalent capacitance of the interface is

$$1/C = 1/C_H + 1/C_{ML} + 1/C_{SC}(U) \qquad (3)$$

where $C_{SC}(U)$ is the only bias-dependent capacitance. We used the classical Poisson−Boltzmann approximation for C_{SC}.[5,8] Though this overestimates C_{SC} under strong accumulation,[25] the whole procedure is not significantly affected by this problem since one reaches a saturation capacitance $C_{SAT} = C_H\, C_{ML}/(C_H + C_{ML})$ at sufficiently negative polarization under strong electron accumulation ($C_{SC}(U) \gg C_H$ and C_{ML}). The calculation of curves yields C_{SAT} and the flat band potential U_{FB}. Note that U_{FB} was independently determined from Mott−Schottky plots $1/C^2-U$[26] and that we found an excellent agreement between the two methods. Assuming that C_H is independent of the surface modification, C_{ML} is determined by inverting the expression of C_{SAT} above and using the C_H value derived from a first measurement with a freshly prepared H−Si(111) electrode. The interface energy diagram at the rest potential was built from the measured OCP (open circuit potential) and flat band potential U_{FB}, accounting for the energy difference $\Delta = 0.31$ eV between the Fermi level and the conduction band minimum for 10 Ω cm n-type silicon ($\Delta = kT\ \ln(N_C/N_D)$ with $N_D = 410^{14}$ cm^{-3} and $N_C = 2.810^{19}$ cm^{-3}).

The effective dielectric constant ϵ_{EFF} of the monolayer was calculated using the expression $C_{ML} = \epsilon_{EFF}\ \epsilon_0/d_{CHAIN}$, where d_{CHAIN} is defined by eq 2. Combining the expression of C_{ML} with eq 3 gives

$$1/C_{SAT} = 1/C_H + d/\epsilon_{EFF}\ \epsilon_0 \qquad (4)$$

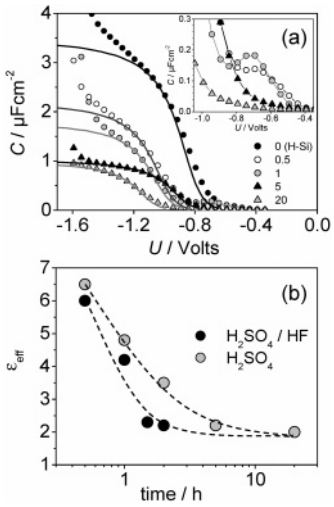

Figure 3. Protocol optimization in the case of Si−C12 samples. (a) $C-U$ plots recorded in 0.1 M H_2SO_4 for increasing reaction times expressed in hours in the figure. Experimental data are symbols, and calculated curves are solid lines. Inset: Enlargement of the region of potential close to the onset of the capacitance rise. (b) Variations of ϵ_{EFF} derived from the fit of $C-U$ plots measured in H_2SO_4 (●) and H_2SO_4/HF (○) as a function of the reaction time.

2.6. X-ray Photoelectron Spectroscopy Measurements. The XPS measurements were performed using a Physical Electronics model 5600 spectrometer modified to average spectra as a function of the azimuth and account for X-ray photodiffraction (XPD) in the comparison of samples. More details are available in ref 24. A monochromatic Al Kα X-ray source and an analyzer pass energy of 12 eV were used. Under these conditions, the overall resolution of the spectrometer is 0.55 eV as measured from the full width at half-maximum of the Ag $3d_{5/2}$ line. The intensity of XPS core levels was measured as the peak area after standard background subtraction according to the Shirley procedure. In the same set of experiments and with the same experimental conditions, we have recorded the Si 2p core level intensity on a reference hydrogen-terminated Si sample and on the modified samples. All spectra were acquired with a take-off angle of 25°, with respect to the surface plane, to maximize surface sensitivity.

3. Results

3.1. Grafting Protocol and Optimization. The protocol was investigated in the case of ≡Si−C12 samples by recording $C-U$ plots in 0.1 M H_2SO_4 after increasing grafting time. Figure 3 shows that all plots (symbols) have the same general shape and that the saturation plateau decreases and becomes better marked as the reaction time increases. The overall plot is also shifting negatively with time. No further evolution is observed after 20 h of grafting. For short reaction times ($t \leq 1$ h) the inset of Figure 3a shows a capacitance peak before the rise of the capacitance (−0.8 V to −0.4 V). After the data were processed, the plots in Figure 3b show a rapid decrease of the effective dielectric constant ϵ_{EFF} with increasing reaction time before reaching a limiting value ∼2.2, in both solutions, a behavior that perfectly agrees with the picture of an organic film progressively covering the silicon surface. The discrepancy between the measurements in the two solutions for reaction times shorter than 2 h is attributed to oxide formation during

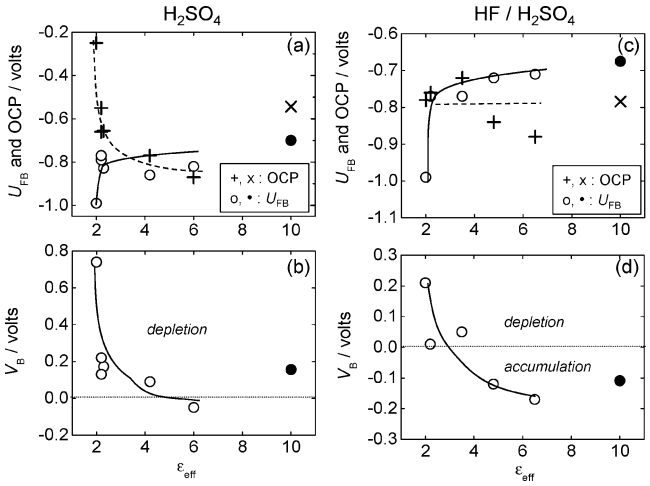

Figure 4. (a and b) Variations of U_{FB} (○) and OCP (+) as a function of ϵ_{EFF} in H_2SO_4 and H_2SO_4/HF solutions. ϵ_{EFF} and U_{FB} are derived from the fit of $C-U$ plots. (c and d) Corresponding variations of the band bending V_B at OCP as a function of ϵ_{EFF}. The values U_{FB} (●) and OCP (×) measured for the H−Si(111) sample have been (arbitrarily) plotted for $\epsilon_{EFF} = 10$.

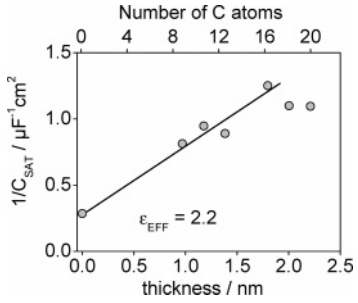

Figure 5. Plot of $1/C_{SAT}$ as a function of d_{CHAIN} (bottom scale) and n (top scale). Equation 2 was used to make the conversion between the two horizontal scales.

or after a *partial* surface modification. In the HF-free solution the oxide affects the capacitance measurement (in the HF-containing solution the oxide is removed). In Figure 4 we have plotted the correlations between the flat band potential U_{FB} (○) and OCP (+) with ϵ_{EFF}. The data points (● and ×) correspond to the case of a freshly prepared H−Si(111) surface with no organic layer (points are arbitrarily placed for $\epsilon_{EFF} = 10$ in the graph). In both solutions, there is a remarkable trend with an abrupt variation of U_{FB} and the OCP when ϵ_{EFF} becomes smaller than a critical value $\epsilon_{EFF}^* \approx 2.5$. The two lower panels in Figure 4 give the variations of the band bending at OCP $V_B = \text{OCP} - U_{FB}$. All these changes will be discussed later.

The optimization of the monolayers consisted of obtaining the smallest possible ϵ_{EFF} and reaching the above-defined U_{FB} and OCP values. As shown in the Supporting Information (Figure S2), we found that the saturation capacitance C_{SAT} decreases with increasing chain length and that the flat band potential is independent of the chain length with a $U_{FB} = -1.0$ V for all monolayers prepared overnight (reaction time ≥ 20 h). Plotting $1/C_{SAT}$ as a function of d_{CHAIN} (Figure 5) provides a direct verification of the equivalent circuit in Figure 2, and the slope of the straight line for $n \leq 16$ yields $\epsilon_{EFF} \approx 2.2$ using eq 4, which is very close to the dielectric constant $\epsilon_{PE} = 2.3$ of polyethylene.[27] This graph confirms therefore that the optimized monolayers with $n \leq 16$ are indeed very dense, which is also in agreement with the XPS data below. It will be justified that ϵ_{EFF} may reach values smaller than ϵ_{PE}. Concerning the data for $n \geq 18$, we noticed that they deviate from the above-mentioned linear law. Two reasons may explain this systematic and reproducible behavior. The first one is the increasing influence of the van der Waals interactions as the chain length increases, which slows down the reaction. (It was not checked whether a longer reaction time would improve packing.) The second reason is the shadowing of free surface sites next to anchored molecules in the course of the reaction. For both reasons C_{ML} is greater than expected because chains with $n \geq 18$ are slightly less densely packed than shorter ones, in agreement with quantitative angle-resolved XPS measurements.[24]

3.2. AFM Observations. A typical AFM image of an optimized Si−C10 modified surface with $\epsilon_{EFF} < \epsilon_{EFF}^* = 2.5$ is displayed in Figure 6a. After reaction in 1-decene the surface looks the same as the starting H−Si(111) surface, with a staircase structure, in which the atomically smooth terraces are separated by a 0.31 nm high step corresponding to one bilayer (BL) of Si(111). Note that the steps are straight over micrometers, because of the precise orientation of the miscut.[22] Prolonged tip scanning does not remove any organic material form the surface, and friction images are featureless, which suggests a uniform molecular coverage on the nanometer scale. The short-range peak-to-peak roughness is 0.06 nm on an individual (111) terrace like on the bare surface. Figure 6b shows that dipping the same sample in 5% HF for 3 min does not alter the surface morphology. One particularly notices that the (111) terraces remain very smooth (roughness 0.12 nm). The only observable change is the disappearance of small white bumps (as pointed out by arrows in Figure 6a) and their replacement by pits with similar sizes (see inside box with enhanced contrast in Figure 6b). The result would be the same after storage of the sample for several weeks in air. In the case of a *nonoptimized* modified surface with $\epsilon_{EFF} \geq \epsilon_{EFF}^*$ the same test (Figure 6c) leads to a profound surface alteration although the initial surface looked like the one in Figure 6a. After the HF treatment, the terrace roughness increases to 0.5 nm, which is about two silicon bilayers (0.62 nm). The array of step edges is nevertheless still recognized. Hence, AFM imaging after a HF rinse appears to be a simple but severe test to assess whether a modified sample is optimized. In the case of the bare surface (not shown) the staircase structure is still well-defined after 7 days in air, and the terrace roughness increases to 0.2 nm on the terraces. The effect of dipping the sample in HF depends then on aging time. A freshly prepared hydrogen-terminated surface dipped in HF keeps its initial staircase structure with no significant increase of the roughness on individual terraces. A 7-day-aged sample leads to generalized terrace roughening (0.3 nm). The positions of the step edges are still visible as in Figure 6c.

The resistance of surfaces against corrosion was investigated by exposing them to 20% NH_4F (with dissolved oxygen). A short HF dip was performed first to remove the oxide clusters (see above). Figure 6d demonstrates that the overall surface topography of an optimized sample with $\epsilon_{EFF} < \epsilon_{EFF}^*$ is remarkably preserved with a terrace roughness that remains as low as 0.12 nm after 30 min in the etching solution. One only notices a few deep pits, whose depths increase with exposure time. This is a manifestation of a *localized* corrosion of the surface from preexisting defects whose origin is discussed below. On the bare surface, the surface is at reverse *generalized*. From a vicinal surface with straight steps (not shown), one obtains a surface with steps of irregular morphology (Figure 6e), which is the signature that the step flow etching is competing with the formation of triangular pits on the terraces,[23] the latter process being promoted by the presence of dissolved

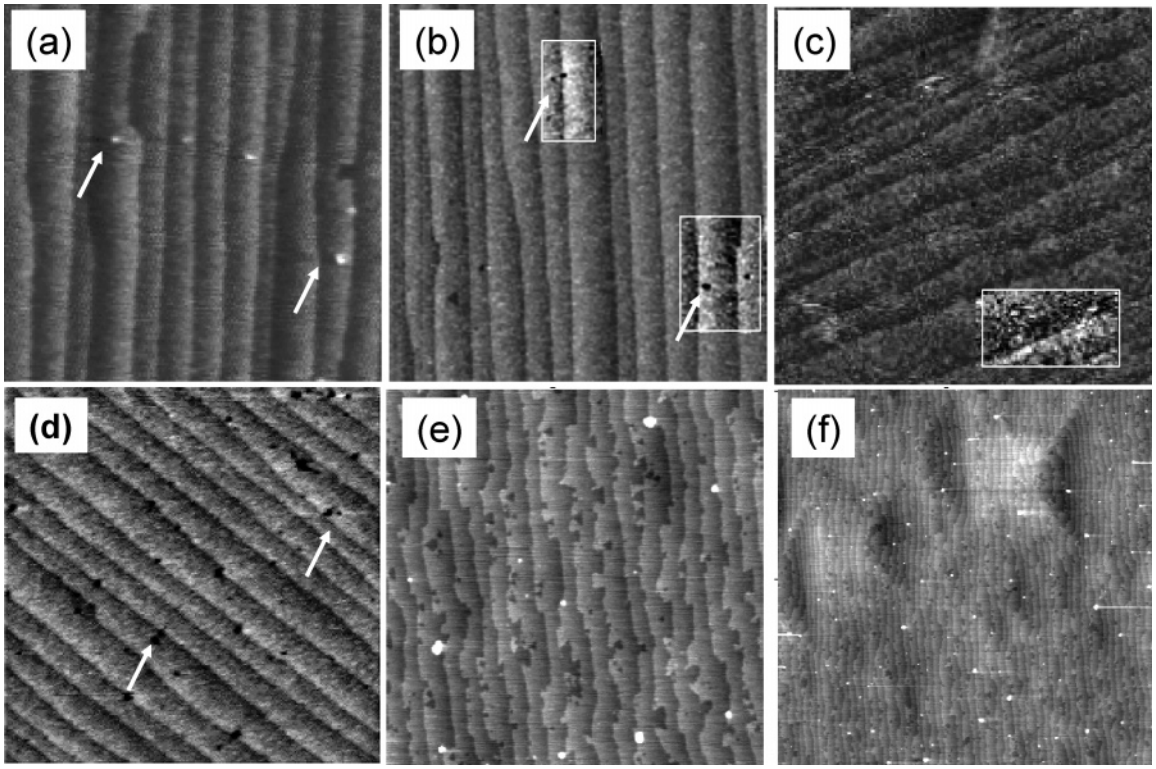

Figure 6. AFM characterizations. (a) Freshly modified Si−C10 surface ($\epsilon_{EFF} \approx 2.2$). (b) Same as part a after a 3 min rinse in 5% HF. Note that the protrusions (arrows) in part a are converted into pits in part b. (See rectangular boxes with image enhanced contrast.) (c) Same as part b but in the case of a less dense Si−C10 monolayer with $\epsilon_{EFF} \approx 5$. Note the increased roughness. (d) Same as part a after 30 min of exposure to 20% NH_4F. (e and f) Same as part d for an initially perfectly stepped hydrogen-terminated surface. All frames are 1×1 μm^2 except part f, which is 5×5 μm^2.

TABLE 1: Physical Characteristics Measured by AFM on Individual (111) Terraces[a]

sample	roughness (nm)	defect height/depth
Hydrogen-Terminated Surface		
as-prepared	0.06	+0.24 nm
as-prepared + HF rinse	0.12	−1 and −2 BL
aged 7 days in air	0.2	not observable
aged 7 days + HF rinse	0.3	not observable
Si−C10 Layer with $\epsilon_{EFF} \approx 2.2$		
as-prepared or aged in air	0.06	+0.24 nm
same + HF rinse	0.12	−1 and −2 BL
exposed to 20% NH_4F	0.12	−2 to −4 BL
Si−C10 Layer with $\epsilon_{EFF} > 2.5$		
as-prepared or aged in air	0.06	+0.24 nm
same + HF rinse	0.50	not observable

[a] The roughness is the short-range peak-to-peak roughness. The defects are the protrusions and pits (typical densities of 10−20 μm^{-2}) observed on all modified and hydrogen-terminated surfaces. The protrusion heights are expressed in nanometers (+), and the depths of the pits (−) are in silicon bilayers (BLs).

oxygen in the 20% NH_4F solution. At a lower magnification (Figure 6f) wide and deep triangular etch pits are resolved, while these are not observed after the initial surface preparation. The first column in Table 1 recalls the roughness on individual terraces, and we infer that the values refer to the Si−molecule interface; the AFM tip is in contact with the silicon surface and is not imaging the top of the molecular layer since the depths of the defects (see next paragraph) are systematically a multiple of a silicon bilayer.

Before closing this section, we will comment on the few nanometer-sized protrusions and pits, which are systematically observed on all samples with sharp enough tips (see arrows in Figures 6a and 6b). Their surface density is typically 10−20 μm^{-2} on every modified or bare surface. The origin of these defects is a *limited* oxidation of the hydrogen-terminated surface *before* grafting. Air oxidation of H−Si(111) is indeed known to occur as a random and progressive nucleation of nanometer clusters.[28] This scheme is consistent with Table 1. Shortly after the surface preparation the oxide cluster density is small, and they are protruding by 0.24 nm over the sample. After 7 days in air their density increases, and the terrace roughness of 0.2 nm suggests that the oxidation is complete, in agreement with XPS (see below). The dip in HF etches away the oxide clusters and leaves nanometer pits in their place because silicon is not dissolved. At the partially oxidized surface, few one-silicon-BL-deep pits are observable, but a complete roughening of the terraces is observed at totally oxidized surfaces. In addition we find that the ratio (protrusion height)/(protrusion height + pit depth) ≈ 0.28−0.4 is close to expectations for selective oxide stripping.[29] From AFM observations we can therefore conclude that the defects (protrusion and pits in Figures 6a and 6b) are not layer defects. Another important issue is that these localized defects cannot be responsible for any of the trends discussed in this study because their equivalent surface coverage is smaller than 1%.

3.3. X-ray Photoelectron Spectroscopy Characterizations of the Optimized Samples. Except for the rise of an intense C 1s peak and the attenuation of the Si 2p peak after the organic modification, there is no difference between the survey XPS spectra of a modified and a bare sample, which could possibly be assigned to the presence of residual aluminum on the modified surface. We hence conclude that if any Al was deposited on the surface, by decomposition of the catalyst upon its neutralization, its surface concentration remains below the detection limit. The absence of Al is also supported by the low density of gap states at the modified interface (see below).

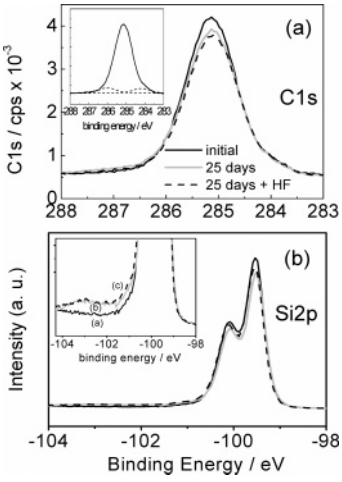

Figure 7. XPS measurements for a Si−C10 modified sample with an optimized monolayer ($\epsilon_{EFF} \approx 2.2$). The take-off angle is 25°. See ref 24 for more experimental details. (a) C 1s core level spectra. Inset: Spectral decomposition showing the two satellite peaks. (b) Si 2p peak. The black, light gray, and dashed lines refer to the as-prepared sample; the peak was the same after 25 day storage in air before and after a final rinse in HF for 3 min. In each case the measurements were performed on the very same sample.

The spectral decomposition and the quantitative analysis of C 1s and Si 2p XPS spectra of an optimized Si−C10 sample were detailed in a recent paper.[24] Here we only give a brief survey of these results and pay attention to the evolution of spectra upon aging in air of a modified and a hydrogen-terminated surface. After the organic modification the C 1s spectrum presents a main component at 285.1 eV, consistent with the grafting of aliphatic chains (Figure 7a, black line). The satellite peaks (see inset) at 284.1 eV are assigned to C−Si bonds[24,30] in accordance with reaction 1. Its relative intensity (~0.07 of the main peak) corresponds to a surface coverage $\theta = 0.45$,[24] which is quite close to the maximum theoretical value of 0.5.[23] The second satellite peak at 286 eV stems from adventitious residual surface contaminations, probably during transfer of the sample through air. Immediately after grafting, the line shape of the Si 2p high-resolution spectra (Figure 7b, black line) is identical to that of the H−Si(111) samples (Supporting Information, Figure S3), and one particularly notices the absence of any component related to oxidized silicon at 103 eV. After 25 days in air, the C 1s spectrum of the modified surface remains unaffected, and only a shallow tail, between 101 and 104 eV, appears in the Si 2p spectrum (light gray line, curve b). A final rinse in HF leaves the C 1s spectrum unchanged. The Si 2p spectrum keeps the same broad and shallow contribution at high binding energy (see inset, dashed curve c). In the control experiment with the bare surface (Supporting Information, Figure S3) a prominent satellite peak (~103 eV) was observed after only 7 days in the air, whose line shape is typical of *compact* SiO_2.

Figure 8a gives the relative variations of the integrated C 1s peak intensity upon aging in air. The data quantitatively show, within experimental uncertainty, that the organic film is intact after 25 days in air, with a variation of the C 1s integrated intensity of only 1%. A significant 6% loss is nevertheless observed after the final HF rinse, meaning that some molecules were removed together with the oxide. Analyzing the variations of the Si 2p spectrum is more subtle and subject to hypothesis because the substrate is buried under the organic film and a growing and discontinuous oxide layer upon aging. To avoid the difficult question of the photoelectron escape depths in these

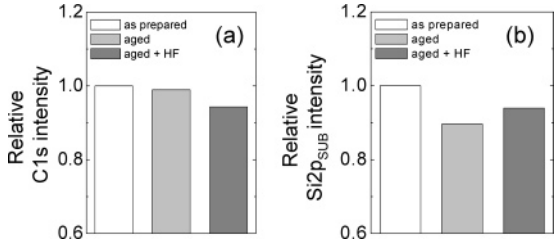

Figure 8. Relative variations of (a) C 1s and (b) Si $2p_{SUB}$ XPS intensities (eq 5). Note the invariance of the C 1s signal intensity upon aging. The variations of Si $2p_{SUB}$ are assigned to oxidation at the interface (see text).

layers, we performed a semiquantitative analysis by decomposing the total Si 2p signal as

$$\text{Si } 2p = \text{Si } 2p_{OX} + \text{Si } 2p_{SUB} \quad (5)$$

The two components Si $2p_{SUB}$ and Si $2p_{OX}$, which correspond, respectively, to photoelectrons emitted from nonoxidized (integration range of 98−101 eV) and oxidized silicon atoms (integration range of 101−104 eV), have been determined from curve fitting. Figure 8b shows that Si $2p_{SUB}$ decreases by 10% after 25 days in air but that the signal intensity is practically restored after the final rinse in HF. This decrease is uniquely correlated with the suboxide uptake observed in the region 101−104 eV in Figure 7b, since we recall that the organic film remains intact during the whole treatment (Figure 8a). The same trend is observed with the uncovered hydrogen-terminated surface, with greater amplitude of variations. After 7 days Si $2p_{SUB}$ decreases by 25% while SiO_2 grows and is restored upon oxide stripping in HF (Supporting Information, Figure S3). The oxide uptake is therefore slowed by the organic layer.

3.4. Monitoring the Interface Properties. The properties of surfaces covered by an optimized decyl ($n = 10$) monolayer of $\epsilon_{EFF} < \epsilon_{EFF}$* were monitored using $C-U$ measurements recorded after exposing the samples to various environments and conditions. In some instances the results obtained with a nonoptimized sample will be shown to outline the role of the molecular surface density. In the case of a dense monolayer with $\epsilon_{EFF} \approx 2.2 < \epsilon_{EFF}$*, very reproducible $C-U$ curves were measured upon repeated cathodic electrode cycling in H_2SO_4 (Figure 9a). A distinct behavior is observed with layers of dielectric constants $\epsilon_{EFF} > \epsilon_{EFF}$*. In this case, the saturation plateau increases (ϵ_{EFF} increases from 4.5 to 5.2), and U_{FB} shifts positively as shown in the inset of Figure 9a. A peak of capacitance is also rising in the potential range -0.95 V $< U < -0.7$ V. After 2.5 months of storage in air the $C-U$ characteristics of an optimized sample remain quasi-unchanged (Figure 9b), and the final HF rinse used to remove eventual oxide has no significant influence. By comparison, the same experiment with a H−Si(111) electrode shows strong alterations of the $C-U$ characteristics with the rise of a prominent capacitance peak in the potential range $-1.15 < U < -0.6$ V (see inset of Figure 9b). This peak is eliminated after the final HF rinse, which proves that it is related to surface oxidation. The flat band potential is also shifted by -0.3 V upon oxidation. The same trends were observed with an unoptimized sample ($\epsilon_{EFF} \approx 5$, not shown). Finally, dipping an optimized sample in 20% NH_4F leaves the $C-U$ plots identical even after 30 min of exposure (Figure 9c). In agreement with AFM observations (Figure 6), the remarkable reproducibility of $C-U$ plots after 30 min of exposure is a further indication that the dissolution of silicon by NH_4F is totally suppressed by the presence of the organic layer except for a residual *localized* dissolution from

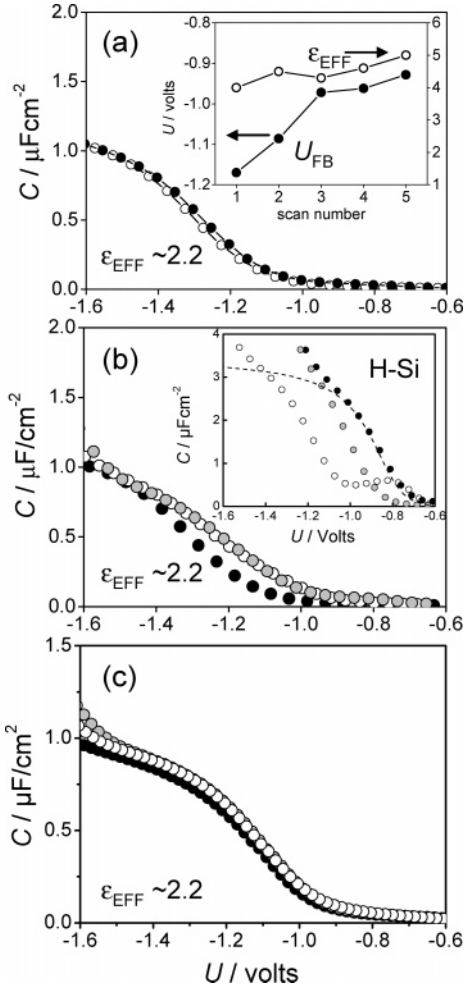

Figure 9. Monitoring of the electronic properties of a ≡Si−C10 electrode with $\epsilon_{EFF} \approx 2.2$ form $C-U$ plots recorded in 0.1 M H_2SO_4. (a) Influence of performing consecutive cathodic cycles. Inset: Evolution of ϵ_{EFF} and U_{FB} for a sample with $\epsilon_{EFF} \approx 4.5$. (b) Influence of storage in air. Inset: Same for a H−Si(111) electrode. Symbols: initial (●), after 2.5 months in air (○), and same plus HF rinse (gray circles). The dotted line is a calculated curve. (c) Influence of the exposure time in 20% NH_4F after a dip in HF: initial (●), 10 min (○), and 30 min (gray circles).

the uncovered parts of the surface, after removal of the few oxide clusters in HF (see deep nanometer pits observed in Figure 6d).

4. Discussion

4.1. Electronic Properties and Chemical Composition at the Interface. The $C-U$ plot of a freshly prepared H−Si(111) sample presents *monotonic* variations, with no peak before the rise of the capacitance (Figure 3 and the inset of Figure 9b). The calculated and the experimental curves are in excellent agreement in the rising part, which means that there are no electronic traps at the surface. (We recall that the calculation assumes that no charge is stored in electronic levels at the silicon surface.[5]) The discrepancy between the calculated and the experimental curves at more negative bias is attributed to electrochemical electron transfer from the conduction band. The absence of gap states at the hydrogen-terminated silicon surface was anticipated because this surface is known to present the slowest recombination velocity ever reported (0.25 cm s^{-1}).[31] Upon storage in air a slow surface oxidation occurs (XPS data in the Supporting Information, Figure S3) with the formation of Si−O−Si bridges on the (111) terraces, which inevitably creates structural defects at the SiO_2/Si(111) interface. The related gap states, which may exchange electrons with the conduction band, are responsible for the prominent capacitance peak in the $C-U$ plots, before the rise of the capacitance (inset of Figure 9b). The filling with electrons of this charge reservoir is also responsible for the negative shift of the $C-U$ plot after oxidation in air. The measured shift $\Delta U_{FB} \approx -0.2$ V corresponds to the storage of $1.2 10^{12}$ electrons/cm^2 using $\Delta Q = C_{SAT} \Delta U_{FB}$ with $C_{SAT} \approx 1\ \mu$F/cm^2. From these correlations, we hence conclude that the gap states must be assigned to surface oxidation. As a supplementary proof we note that the dip in HF, which restores the hydrogen termination of the surface, suppresses the above electronic states and the related peak of capacitance.

In analogy with the above reasoning, we readily deduce that an optimized modified sample presents also a low density of gap states because the $C-U$ curve presents no capacitance peak (Figure 9). The very good agreement between the calculated (solid lines) and the experimental plots in Figure 3 supports this conclusion Because the electrode is at thermodynamic equilibrium (see below), we derive from the band diagram at OCP an interface defect density of $\sim 3.3 10^{10}$ defects/cm^2,[32] which represents only one surface defect every 20 000 atoms, if one assumes one electron per site. This is an extremely low density of defects. This is also hardly measurable with surface techniques. Such a remarkable result is assigned to the structure of the interface silicon−organic layer, which is free of defects, since it is composed of Si−C and Si−H bonds (XPS data, Figures 7 and 8). Moreover these bonds are only weakly polarized. Our estimate is consistent with the $\sim 10^{10}$ traps/cm^2 estimated by others for a Si(100) surface treated in I_2/methanol to create Si−O−CH_3 termination.[33] A small density of states was also inferred from the slow recombination velocity measured at silicon surfaces modified with benzyl rings.[9] Others have reported relatively small recombination velocities (∼30−500 cm s^{-1}).[34,35] Upon storage in air the modified surface is partially oxidized at a slower rate than the bare surface. In addition after 25 days in air suboxide rather than compact oxide forms as shown by the distribution of oxidation states $Si^+ < Si < Si^{4+}$ in the Si 2p spectrum (Figure 7b). Despite an obvious suboxide formation upon prolonged storage in air, the density of gap states remains very low if one considers the small shift of U_{FB} (Figure 9b). Suboxide species are mostly silanol groups Si−OH (Si^+) because these surface sites do not promote deep electronic traps, in analogy with the low trap density found at the Si−O−CH_3 surface.[33] A low density of states explains also that the capacitance peak is less prominent at the aged modified surface than at the oxidized bare surface (Figure 9b).

4.2. Energy Diagram of the Interface: A Sensitive Criterion. As mentioned above, the data indicate that dense monolayers are obtainable because the dielectric constant is close to that of polyethylene after optimization. This primary criterion, immediately derived from the $C-U$ curves, is completed by Figure 10 in which we display the energy diagrams of the interface at rest potential for the hydrogen-terminated (parts a and c) and an optimized Si−C10 sample (parts b and d). These diagrams were constructed after the data given in Figure 4. For a nonoptimized Si−C10 sample the situation would be intermediate but somewhat closer to that of the hydrogen-terminated surface. The remarkable evolution of the diagram after the surface modification can be rationalized by considering the cathodic hydrogen evolution reaction (J_{HER}), the anodic silicon electrochemical dissolution or oxidation (J_{DISS}, J_{OX}), and the space charge recombination (J_{SCR}), which is occurring inside

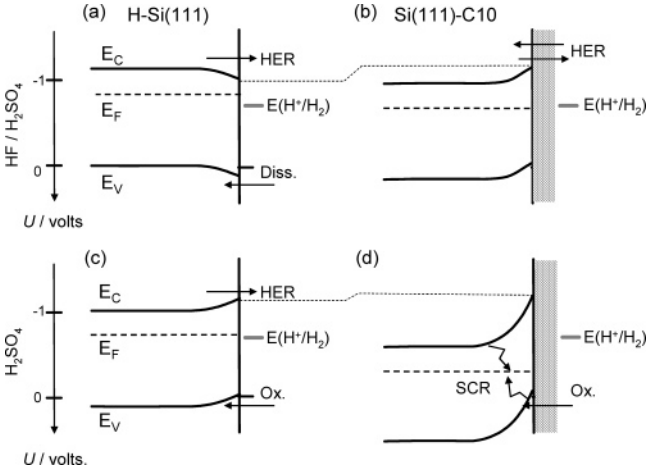

Figure 10. Energy diagram of a hydrogen-terminated (a and c) and of an optimized modified (b and d) n-type Si(111) electrode at OCP in H_2SO_4/HF (a and b) and in H_2SO_4 (c and d). The diagrams were built after the data in Figure 4. The H^+/H_2 redox level is shown in each case. Arrows show the flow of electrons *J* responsible for equilibrium. The suffixes refer to hydrogen evolution reaction (HER), silicon dissolution (DISS), silicon oxidation (OX), and space charge recombination processes (SCR).

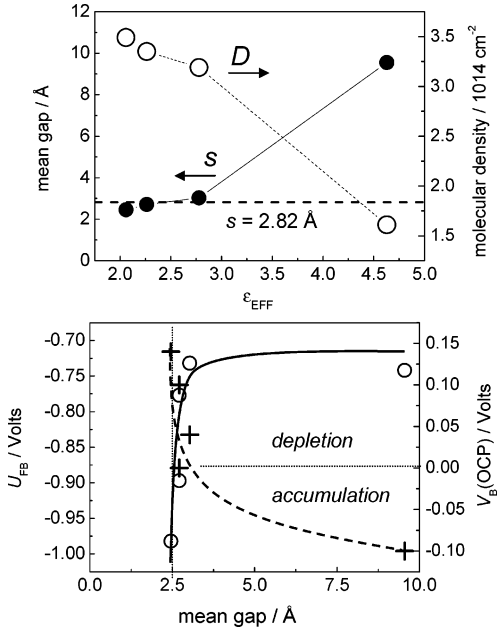

Figure 11. (a) Plot of the channel diameter *s* (●) and molecular density *D* (○) as a function of the *experimental* value of ϵ_{EFF}. The curves were constructed using the plot chart in Figure A2b. (b) Plots of U_{FB} (○), V_B (+) as a function of *s*. Note the abrupt variations around $s \approx 2.8$ Å.

the electrode. In each situation, we only indicate the dominating processes, and the direction of arrows refers to the direction of electron flow.

In the HF-containing solution the electrochemical equilibrium arises only from the balance $J_{HER} = J_{DISS}$ at the bare surface (Figure 10a). The equilibrium is dynamic and not thermodynamic since the two Fermi levels of the two phases are not equal. It is worth noticing that electrons are accumulated at the surface to compensate for the silicon dissolution, which is a sign that the kinetics of the HER is slow. The HER reaction is especially slow at a *well-defined* stepped hydrogen-terminated surface because this surface offers a small density of favorable atomic sites. (The HER involves the desorption of H atoms from the step edges.[36]) After the surface modification, the dissolution is totally suppressed, as demonstrated by the test in NH_4F (Figures 6d and 9c), and a quasi-perfect thermodynamic equilibrium establishes with the H^+/H_2 redox couple (arrows in Figure 10b). In the H_2SO_4 solution the hydrogen termination of the bare surface evolves progressively toward an oxidized state (J_{OX}) despite the fact that the solution was carefully outgassed. Thermodynamic equilibrium is almost satisfied because the oxide formation blocks electron transfer, which is equivalent to reduce the corrosion current in part a (Figure 10c). After the organic modification the interface resists against oxidation in H_2SO_4 (Figure 10d), and maximum depletion is observed. (The silicon Fermi level lies very close to the top of the valence band maximum at the surface.) We infer that the residual oxidation current becomes extremely small and that electron transfer is totally blocked. A residual current flows, however, which is equal to J_{SCR}. The magnitude of J_{SCR} is an intrinsic property of the silicon wafer.[37]

The construction of the interface energy diagram provides therefore a refined criterion to assess whether a modified sample is optimized or not. To be considered as truly optimized, a modified sample should present (i) a dielectric constant $\epsilon_{EFF} < \epsilon_{EFF}^* \approx 2.5$, (ii) a flat band potential shifted negatively with respect to that of the bare surface, and (iii) a band bending while $V_B > 0$ in the HF-containing solution or in H_2SO_4. It is worth noticing that the above results are general and are not specific to the alkyl layers. We also find that optimized alkoxy monolayers and acid-terminated alkyl layers present similar energy diagrams in acidic solutions.

4.3. Interpretation of the ϵ_{EFF}^* Value. The above results have shown that the dielectric constant must be smaller than a threshold value ϵ_{EFF}^* to ensure a long-term passivation of the interface characteristics. To give a physical origin to the value of ϵ_{EFF}^*, the experimental data ϵ_{EFF}−reaction time shown in Figure 3 have been replotted as $s-\epsilon_{EFF}$ and $D-\epsilon_{EFF}$ plots in Figure 11a, with *s* the intermolecular channel diameter and *D* the molecular surface density, using the chart plot $\epsilon_{EFF}-D$ given in the Appendix (Figure A2b). We have also replotted U_{FB} and V_B as a function of *s* in Figure 11b. The salient point of these two graphs is that the curve $s-\epsilon_{EFF}$ intercepts the horizontal line $s = d_{WATER} = 2.82$ Å[38] for $\epsilon_{EFF} \approx 2.5$. There is also a close coincidence between the sharp decrease of U_{FB} around $s \approx d_{WATER}$. At the same time V_B changes sign to become positive in the HF solution (i.e., the n-type silicon is under depletion).

According to the geometrical model in the Appendix, such ideal monolayers are densely packed monolayers, with a molecular density above a critical surface density $D_C \approx 3.3 \times 10^{14}$ cm^{-2} or, equivalently, a mean diameter of intermolecular channels narrower than the hard sphere diameter of water molecules ($d_{WATER} \approx 2.82$ Å[38]). The corresponding value of the surface coverage $\theta > 0.42$ is in close agreement with the value derived from XPS data for optimized samples.[24] We can therefore safely conclude that long-term passivation of the hybrid interface arises from the exclusion of water from the organic monolayer at the nanometer scale. Under this key condition air oxidation is remarkably retarded over weeks and months (Figure 9b). Repeated cathodic polarization has no effect (Figure 9a), and more remarkable, the dissolution of silicon was strongly inhibited for tens of minutes in 20% NH_4F (Figures 9c and 6d).

5. Conclusion

We have prepared Si(111)−alkyl layer interfaces with a very low density of electronic traps (few 10^{10} traps/cm^2) after careful control of the grafting conditions. The cross correlations between

XPS data and $C-U$ plots demonstrate that the electrochemical measurements constitute a powerful tool to characterize and monitor the chemical state of the interface and the molecular density of the organic monolayer as a function of the treatment. The construction of the energy diagram of the optimized interface, which differs remarkably from that of the bare surface, gives complementary information, and the method seems to be even more sensitive to the film structure than the simple measurement of ϵ_{EFF}. Using this technique we have found that a very long reaction ($\geq$20 h) time is required to preserve the integrity of the interface over the long term in air and some aqueous solutions. Thanks to a simple model, we have demonstrated that the cutoff value $\epsilon_{EFF} = 2.5$ is related to water exclusion at the nanometer scale. This situation corresponds to layers with a surface density $D > 3.3 \times 10^{14}$ chains/cm^2 or a surface coverage $\theta > 0.42$.

Acknowledgment. P.G. acknowledges financial support from the Direcció General de Recerca of the Generalitat de Catalunya (Fellowship No. 1999-BEAI-200457).

Appendix

The model below establishes a relationship between the dielectric constant capacitance ϵ_{EFF} and the molecular surface density D. Figure A1 shows a top view of the silicon surface with 50% occupancy and the corresponding cross section AA′. The rectangular array is $a = 3.84$ Å $\times$ $b = 6.65$ Å as in Figure 1b, which corresponds to $(1 \times \sqrt{3})$R30° surface structure (unit cell area 25.6 Å^2). The maximum theoretical packing density on Si(111) is therefore $D_{MAX} = 3.9\ 10^{14}$ molecules/cm^2. The tilted rectangles in the cross section BB′ stand for the *projection on the image plane* of rows of aliphatic chains. Each chain is a cylindrical rigid rod of length L and ellipsoidal section ($2c_1 = d = 1/\sqrt{D_{PE}} = 4.61$ Å and $2c_2 = 3.84$ Å). The tilt is $\alpha = 35.5°$ as in Figure 1a. In this scheme the rods may eventually rotate around the first C carbon atom involved in the Si−C bond. The rotation center is the first C atom at $d_0 = 1.89$ Å from the silicon surface. The surface unit cell is $(a \times b)$, and the molecular density $D = 10^{16}/(a \times b)$, where a and b are expressed in angstroms.

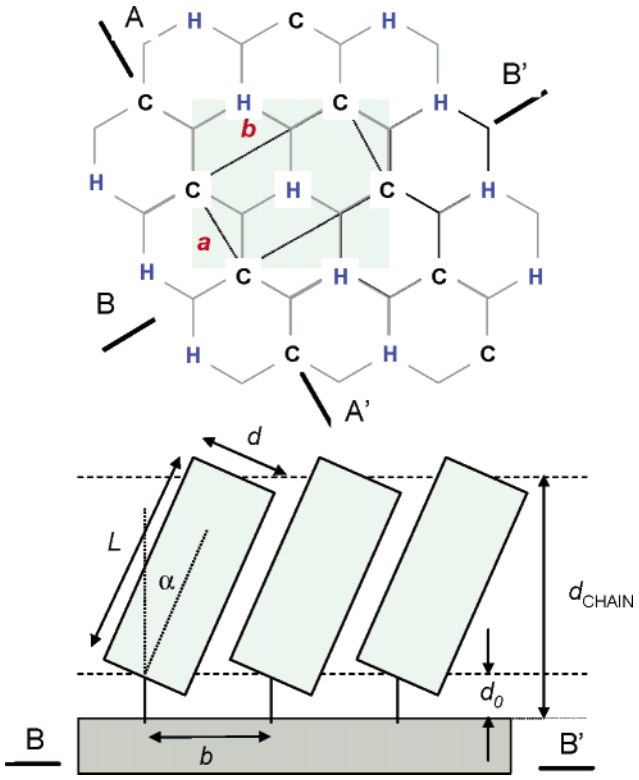

Figure A1. Geometrical model used to calculate the volume fraction occupied by the molecules in the monolayer. (a) Top view of the Si-(111) surface in which the C sites are Si−H moieties that were substituted by a molecular chain. The rectangular unit cell ($a = 3.84$ Å $\times$ $b = 6.65$ Å) corresponds to a surface coverage of 0.5. (b) BB′ cross section of the interface. The rectangles are the projections of rows of the aliphatic chains, considered as cylinders of length L and ellipsoidal sections ($c_1 = a/2$, $c_2 = d/2$, with $d = 4.61$ Å). For a close packed layer $b = 6.65$ Å and increases for less dense monolayers. See text for the determination of the mean diameter of the intermolecular channel. d_{CHAIN} and d_O are defined by eq 2.

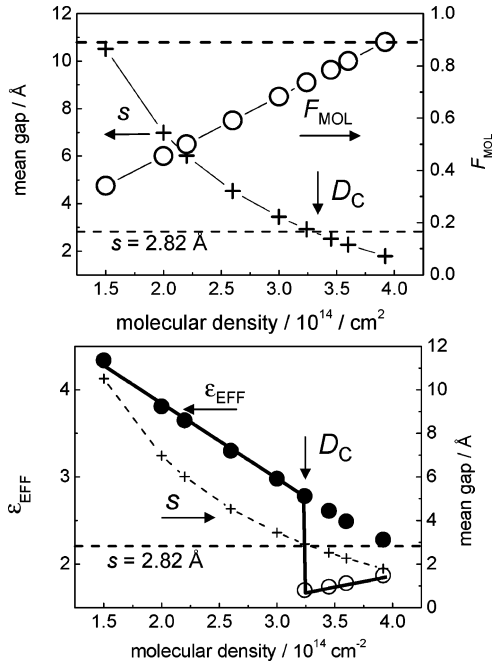

Figure A2. (a) Plots of s and F_{MOL} as a function of D. (b) Calculated plots of ϵ_{EFF} as a function of D in the case where $\epsilon_M = 1$ (○) and 6 (●). The solid line is the theoretical plot $\epsilon_{EFF}-D$ upon opening of the intermolecular channels. The abrupt jump coincides with the value $s = 2.82$ Å.

To account for the variations of D in the course of the grafting reaction, we vary b continuously in the expression of D above and keeping $a = 3.84$ Å since the close packing along AA′ is easier for steric reasons. Under this assumption, b stands now for the *mean* distance between neighboring rows of rods along the axis BB′ ($b = 6.65$ Å in the case of a perfect $1 \times \sqrt{3}$ structure). The volume fraction occupied by the aliphatic chains in the layer is $F_{MOL} = (D/\cos(\alpha))/D_{PE}$, where $D_{PE} = 5.4 \times 10^{14}$ molecules/cm^2 is the chain density in crystallized polyethylene[39] and the $\cos(\alpha)$ accounts for the chain tilt from the surface normal. Through simple geometry, a mean diameter s was calculated for the channel between the molecular chains. Figure A2a plots the variations of s (+) and F_{MOL} (○) as a function of D. The upper limit of F_{MOL} is 0.892 when $D = D_{MAX}$. The intercept between the plot $D-s$ with the dashed horizontal line $s = d_{WATER}$, where $d_{WATER} = 2.82$ Å is the hard sphere diameter of molecular water,[38] defines a critical density $D_C \approx 3.3 \times 10^{14}$ cm^{-2} below which the channels between the molecules are smaller than d_{WATER}. In such a situation molecular water is excluded from the organic monolayer.

The theoretical ϵ_{EFF} was calculated from the above $F_{MOL}-s$ plot using the Bruggeman effective medium theory formalism[40]

$$F_{MOL}\{\epsilon_{MOL} - \epsilon_{EFF}\}/\{\epsilon_{MOL} + 2\epsilon_{EFF}\} + (1 - F_{MOL})\{\epsilon_M - \epsilon_{EFF}\}/\{\epsilon_M + 2\epsilon_{EFF}\} = 0$$

This equation was solved with the dielectric constant of molecules $\epsilon_{MOL} = 2.3$. Two cases were considered for the dielectric of the foreign medium: $\epsilon_M = 1$ if air is trapped between the chains and $\epsilon_M = 6$ if molecular water is trapped between the chains.[41] Figure A2b gives the variations of ϵ_{EFF} with D when $\epsilon_M = 1$ (○) and $\epsilon_M = 6$ (●). The dependence of s with D (− + −) is also plotted. When $s < d_{WATER}$ or $D > D_C$ it is justified to consider the curve $\epsilon_{EFF}-D$ calculated with $\epsilon_M = 1$ since water cannot penetrate inside the organic layer (air is trapped). When $s > d_{WATER}$ or $D < D_C$ water may be incorporated into the monoloayer, and the curve $\epsilon_{EFF}-D$ calculated with $\epsilon_M = 6$ must be considered. Bridging the two cases gives the solid line $\epsilon_{EFF}-D$ as the theoretical variations of ϵ_{EFF} over a wide range of surface density D. This plot was used to convert the experimental value ϵ_{EFF} of Figure 3 into a surface density D and into a gap s.

Supporting Information Available: $C-U$ plots recorded with a Si−C10 sample in 0.1 M H_2SO_4 at different frequencies from 1 kHz to 10 kHz, chain length dependence of the $C-U$ plots recorded in 0.1 M H_2SO_4 at a measurement frequency of 1 kHz and the chain length indicated, normalized Si 2p XPS spectra of a H−Si(111) sample stored in air to show the progressive oxide uptake, and relative variations of the peak intensity (integrated between 98 and 101 eV). This material is available free of charge via the Internet at http://pubs.acs.org.

References and Notes

(1) For a review see: Wayner, D. D. M.; Wolkow, R. A. *J. Chem. Soc., Perkin Trans. 2* **2002**, 23.

(2) For a review see: Buriak, J. *Chem. Rev.* **2002**, *102*, 1271.

(3) Boukherroub, R.; Morin, S.; Sharpe, P.; Wyaner, D. D. M.; Allongue, P. *Langmuir* **2000**, *16*, 7429.

(4) (a) Ulmann, A. *Chem. Rev.* **1996**, *96*, 1533. (b) Love, J. C.; Estroff, L. A.; Kriebel, J. K.; Nuzzo, R. G.; Whitesides, G. M. *Chem. Rev.* **2005**, *105*, 1103.

(5) Allongue, P.; Henry de Villeneuve, C.; Cherouvrier, G.; Cortes, R. *J. Electroanal. Chem.* **2003**, *550−551*, 161.

(6) Nihonyanagi, S.; Miyamoto, D.; Idojiri, S.; Uosaki, K. *J. Am. Chem. Soc.* **2004**, *126*, 7034.

(7) Poirier, G. E. *Chem. Rev.* **1997**, *97*, 1117.

(8) Allongue, P.; Henry de Villeneuve, C. *Electrochim. Acta* **2000**, *45*, 3241.

(9) Hartig, P.; Dittrich, Th.; Rappich, J. *J. Electroanal. Chem.* **2002**, *524*, 120.

(10) For a review see: (a) Bergveld, P. *Sens. Actuators, B* **2003**, *88*, 1. (b) Schoning, M.; Poghossian, A. *Analyst* **2002**, *127*, 1137.

(11) Sze, S. M. In *Physics of Semiconductor Devices*; Wiley & Sons: New York, 1969.

(12) Linford, M. R.; Chidsey, C. E. D. *J. Am. Chem. Soc.* **1993**, *115*, 12631.

(13) Linford, M. R.; Fenter, P.; Eisenberger, P. M.; Chidsey, C. D. E. *J. Am. Chem. Soc.* **1995**, *117*, 3145.

(14) Buriak, J. M.; Stewart, M. P.; Geders, T. W.; Allen, M. J.; Choi, H. C.; Smith, J.; Raftery, D.; Canham, L. T. *J. Am. Chem. Soc.* **1999**, *121*, 11491.

(15) Sieval, A. B.; Demirel, A. L.; Nissink, J. W. M.; Linford, M. R.; van der Maas, J. H.; de Jeu, W. H.; Zuilhof, H.; Sudhölter, E. J. R. *Langmuir* **1998**, *14*, 1759.

(16) Boukherroub, R.; Bensebaa, F.; Morin, S.; Wayner, D. D. M. *Langmuir* **1999**, *15*, 3831.

(17) Bateman, J. E.; Eagling, R. D.; Worrall, D. R.; Horrocks, B. R.; Houlton, A. *Angew. Chem., Int. Ed.* **1998**, *37*, 2683.

(18) Cicero, R. L.; Linford, M. R.; Chidsey, C. E. D. *Langmuir* **2000**, *16*, 5688.

(19) Jin, H.; Kinser, C. R.; Bertin, P. A.; Kramer, D. E.; Libera, J. A.; Hersam, M. C.; Nguyen, S. T.; Bedzyk, M. J. *Langmuir* **2004**, *20*, 6252.

(20) Fellah, S.; Teyssot, A.; Ozanam, F.; Chazalviel, J.-N.; Vigneron, J.; Etcheberry, A. *Langmuir* **2002**, *18*, 5851.

(21) Yu, H.-Z.; Morin, S.; Wayner, D. D. M.; Allongue, P.; Henry de Villeneuve, C. *J. Phys. Chem. B* **2000**, *104*, 11157.

(22) (a) Munford, M. L.; Cortès, R.; Allongue, P. *Sens. Mater.* **2001**, *13*, 259. (b) Allongue, P.; Henry de Villeneuve, C.; Morin, S.; Boukherroub, R.; Wayner, D. D. M. *Electrochim. Acta* **2000**, *45*, 4591.

(23) Sieval, A.; van der Hout, B.; Zuilhof, H.; Sudhölter, E. J. R. *Langmuir* **2001**, *17*, 2172.

(24) Wallart, X.; Henry de Villeneuve, C.; Allongue, P. *J. Am. Chem. Soc.* **2005**, *127*, 7871.

(25) Allongue, P.; Henry de Villeneuve, C.; Ozanam, F.; Chazalviel, J.-N., manuscript in preparation.

(26) Morrison, S. R. In *Electrochemistry at Semiconductor and Oxidized Metal Electrodes*; Plenum Press: New York, 1980.

(27) Lanza, V. L.; Herrman, D. B. *J. Polym. Sci.* **1958**, *28*, 622.

(28) Neuwald, U.; Hessel, H.; Feltz, E. A.; Memmert, U.; Behm, R. J. *Appl. Phys. Lett.* **1992**, *60*, 1307.

(29) Avouris, Ph.; Martel, R.; Hertel, T.; Sandstrom, R. *Appl. Phys. A* **1998**, *66*, S659.

(30) (a) Liu, H.; Hamers, R. J. *Surf. Sci.* **1998**, *416*, 354. (b) Liu, Z. H.; McCaffrey, J. P.; Brar, B.; Wilk, G. D.; Wallace, R. M.; Feldman, L. C.; Tay, S. P. *Appl. Phys. Lett.* **1997**, *71*, 2764.

(31) Yablonovitch, E.; Allara, D. L.; Chang, C. C.; Gmitter, T.; Bright, T. B. *Phys. Rev. Lett.***1986**, *57*, 249.

(32) The modified interface is at thermodynamic equilibrium at OCP in the HF-containing solution (Figure 4). The surface charge is therefore equal to the space charge inside the silicon. Writing $Q_S = W N_D$, where $W = (2\epsilon\epsilon_0/eN_D)^{1/2}V_B^{1/2}$ is the width of the space charge layer[26] and N_D is the doping level. Numerical application yields a charge Q_S as low as 7.310^9 electron per cm^2 using $\epsilon = 11.9$, $N_D = 410^{14}$ cm^{-3} and $V_B = 0.2$ V. Assuming that each defect bears only one elementary charge, the defect density is ca. 3.310^{10} cm^{-2} or one atomic defect every 2.10^4 surface atoms.

(33) Reddy, A. J.; Chan, J. V.; Burr, T. A.; Mo, R.; Wade, C. P.; Chidsey, C. E. D.; Mitchel, J.; Kimerling, L. M. *Physica B* **1999**, *273−274*, 468.

(34) Sieval, A. B.; Huisman, C. H.; Schönecker, A.; Schuurmans, F. M.; van der Heide, A. S. H.; Goosens, A.; Sinke, W. C.; Zuilhof, H.; Sudhölter, E. J. R. *J. Phys. Chem. B* **2003**, *107*, 6846.

(35) Webb, L. J.; Lewis, N. S. *J. Phys. Chem. B* **2003**, *107*, 5404.

(36) Allongue, P.; Costa-Kieling, V.; Gerischer, H. *J. Electrochem. Soc.* **1993**, *140*, 1018.

(37) Rosenbluth, M. L.; Lewis, N. S. *J. Am. Chem. Soc.* **1986**, *108*, 4689.

(38) (a) Urquidi, J.; Singh, S.; Cho, C. H.; Robinson, G. W. *Phys. Rev. Lett.* **1999**, *83*, 2348. (b) Cho, C. H.; Singh, S.; Robinson, G. W. *J. Chem. Phys.* **1983**, *107*, 7979.

(39) Dorset, D. L. *J. Phys. Chem. B* **2000**, *104*, 8346.

(40) Theiss, W. *Surf. Sci. Rep.* **1997**, *89*, 91.

(41) $\epsilon \approx 6$ is the accepted value for the first monolayer of molecular water at the electrode surface. See Bockris, J. O'M.; Reddy, A. K. N. In *Modern Electrochemistry*; Plenum Press: New York, 1970.